

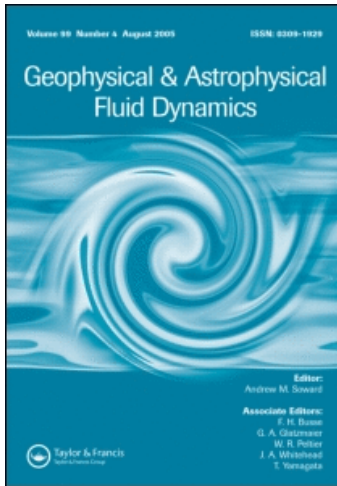
This article was downloaded by: [Lapeyre, Guillaume]

On: 24 December 2010

Access details: Access Details: [subscription number 931550679]

Publisher Taylor & Francis

Informa Ltd Registered in England and Wales Registered Number: 1072954 Registered office: Mortimer House, 37-41 Mortimer Street, London W1T 3JH, UK



Geophysical & Astrophysical Fluid Dynamics

Publication details, including instructions for authors and subscription information:

<http://www.informaworld.com/smpp/title~content=t713642804>

Ocean turbulence at meso and submesoscales: connection between surface and interior dynamics

Patrice Klein^a; Guillaume Lapeyre^b; Guillaume Roulet^a; Sylvie Le Gentil^a; Hideharu Sasaki^c

^a LPO/CNRS/IFREMER, BP70 IFREMER, Plouzane, France ^b LMD/ENS/IPSL/CNRS, Paris, France ^c

Earth Simulator Center, Yokohama, Japan

First published on: 23 December 2010

To cite this Article Klein, Patrice , Lapeyre, Guillaume , Roulet, Guillaume , Gentil, Sylvie Le and Sasaki, Hideharu(2010) 'Ocean turbulence at meso and submesoscales: connection between surface and interior dynamics', Geophysical & Astrophysical Fluid Dynamics,, First published on: 23 December 2010 (iFirst)

To link to this Article: DOI: 10.1080/03091929.2010.532498

URL: <http://dx.doi.org/10.1080/03091929.2010.532498>

PLEASE SCROLL DOWN FOR ARTICLE

Full terms and conditions of use: <http://www.informaworld.com/terms-and-conditions-of-access.pdf>

This article may be used for research, teaching and private study purposes. Any substantial or systematic reproduction, re-distribution, re-selling, loan or sub-licensing, systematic supply or distribution in any form to anyone is expressly forbidden.

The publisher does not give any warranty express or implied or make any representation that the contents will be complete or accurate or up to date. The accuracy of any instructions, formulae and drug doses should be independently verified with primary sources. The publisher shall not be liable for any loss, actions, claims, proceedings, demand or costs or damages whatsoever or howsoever caused arising directly or indirectly in connection with or arising out of the use of this material.

Ocean turbulence at meso and submesoscales: connection between surface and interior dynamics

PATRICE KLEIN^{†*}, GUILLAUME LAPEYRE[‡], GUILLAUME ROULLET[‡],
SYLVIE LE GENTIL[†] and HIDEHARU SASAKI[§]

[†]LPO/CNRS/IFREMER, BP70 IFREMER, Plouzane, France

[‡]LMD/ENS/IPSL/CNRS, Paris, France

[§]Earth Simulator Center, Yokohama, Japan

(Received 30 January 2010; in final form 4 May 2010)

High resolution simulations of ocean turbulence with Rossby number of order one have revealed that upper layer dynamics significantly differs from the interior dynamics. As reported before, upper layer dynamics is characterized with shallow velocity spectrum corresponding to kinetic energy distributed over a spectral range from mesoscales to small scales. This dynamics is driven by small-scale frontogenesis related to surface density anomalies. Interior dynamics is characterized by steeper velocity spectrum and is driven by the potential vorticity anomalies set up by the interior baroclinic instability. Impact of the divergent motions related to surface frontogenesis leads to a warming of the upper layers, a cyclone dominance and a negative skewness of the isopycnal displacements. On the contrary, divergent motions in the interior lead to a cooling of the deeper layers, an anticyclone dominance and a positive skewness of the isopycnal displacements. These different ageostrophic processes are consistent with an SQG regime extended to Rossby number of order one on one hand and an interior QG regime extended to Rossby number of order one on the other hand, as proposed by previous studies. Synthesis of these characteristics suggest a connection between upper and deeper layers, induced by the divergent motions, through which small scales near the surface interact with mesoscales in the interior.

Keywords: Ocean turbulence; Ageostrophic effects; Boundary-interior connection

1. Introduction

Ocean turbulence, that includes mesoscale (100–300 km) oceanic eddies and sub-mesoscale structures (such as elongated filaments with a width of 10–50 km), has been fully uncovered by multifaceted satellite data (figures 1(a) and (b)). Global altimeter data have revealed that mesoscale eddies are present in large numbers in all oceans in particular at mid-latitudes (Chelton *et al.* 2007). These eddies, whose depth extension reaches 500–1000 m, are also well reproduced by the present Ocean Global Climate models (OGCM) with a resolution of 1/10th degree and are known to have strong impacts onto the large-scale ocean circulation (Smith *et al.* 2000) and on the

*Corresponding author. Email: patrice.klein@ifremer.fr

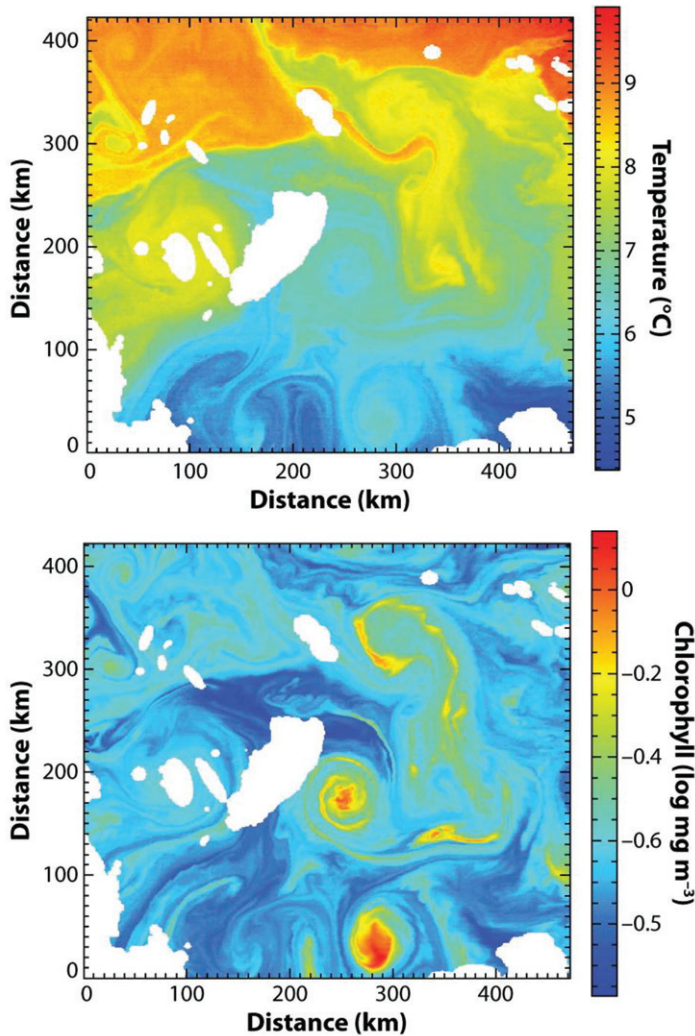


Figure 1. SST and ocean color images from satellite data, at the same time and location, revealing the signature of mesoscale eddies and submesoscale structures (Jordi Isern-Fontanet: personal communication).

biogeochemical system (McGillicuddy *et al.* 1998). Such eddies are driven by the potential vorticity (PV) anomalies in the ocean interior set up by the baroclinic instability and their properties are close to the quasi-geostrophic (QG) properties (involving a velocity spectrum slope in k^{-3} to k^{-4}) (Smith and Vallis 2002). Submesoscales are present only in the high resolution infrared and color satellite images that unfortunately do not provide any dynamical information. These structures, insufficiently resolved by the present OGCM, have been thought for a long time to be passively stretched by mesoscale eddies (Abraham *et al.* 2000) with no dynamical impact on the ocean circulation. However, recent Primitive Equations (PE) simulations with high resolution (1/100th degree) have revealed that these submesoscales are much more energetic than previously thought, in particular in the first 300 m (Capet *et al.* 2008a, Klein *et al.* 2008). They have been found to explain more than 50% of the

vertical velocity field in these layers (Klein *et al.* 2008). These high resolution simulations further showed that the surface dynamics is characterized by a Rossby number of order one and a k^{-2} velocity spectrum slope over a large scale range including mesoscales. Such spectral properties, conspicuously close to surface quasi-geostrophic (SQG) properties (Blumen 1978), have been confirmed recently by a reanalysis using several altimeter data sets (Le Traon *et al.* 2008).

The analytical diagnosis by Lapeyre and Klein (2006) (LK06) and Tulloch and Smith (2006) of the ocean dynamics in terms of surface and interior properties within the QG framework anticipate some of the results from these high resolution simulations and in particular suggested a one-way interaction of mesoscale eddies onto the surface-trapped submesoscales. Indeed, results of these two papers suggest that, in the surface layers, small scales are mostly driven by the SQG dynamics (i.e. the surface frontogenesis associated with the small-scale surface density anomalies), whereas mesoscales present at the surface are driven by the interior QG dynamics. Tulloch and Smith (2009) further determine that the frontier between both scale ranges is located at a scale close to the Charney scale. Since surface-trapped submesoscales result from the direct cascade of surface density variance that is driven by mesoscale motions, this indicates a one-way interaction of the interior dynamics onto the surface dynamics.

However, and it is the purpose of this article, a detailed analysis of these recent high resolution PE simulations rather indicates a two-way connection between surface and interior dynamics. As mentioned in the following sections, this is due to the energetic divergent motions. As a result surface trapped submesoscales may affect the dynamics of mesoscale eddies with larger depth extension and, therefore, the interior dynamics. Furthermore, through these divergent motions, small-scale surface frontogenesis (that transforms available potential energy (APE) into kinetic energy (KE)) feeds up the inverse KE cascade at the surface and, therefore, increases the KE of mesoscale eddies.

After a brief description of the recent high resolution PE simulations in section 2, section 3 reviews the surface and interior properties revealed by these simulations. Then section 4 discusses the two-way connection between surface and interior dynamics that emerges from these properties. Conclusions are offered in section 5.

2. Simulations of ocean turbulence with high 3-D resolution

Recent numerical PE simulations of a nonlinear baroclinic unstable oceanic flow in a zonal β -plane channel centered at 45°N (Rivi re *et al.* 2004) have been performed at high resolution and are fully described in Klein *et al.* (2008). The domain size is $1000\text{ km} \times 2000\text{ km}$ and its depth 4000 m . The numerical resolution is 1 km in the horizontal and 200 levels on the vertical (vertical grid spacing ranges from 1.5 m near the surface to 100 m near the bottom). The Brunt-V is l a frequency profile corresponds to a main thermocline located at a depth around 600 m and corresponds to a first Rossby radius of deformation of approximately 30 km . The initial state consists of an unstable large-scale meridional density gradient that is surface intensified. The mesoscale and sub-mesoscale eddy turbulence is forced by using a relaxation of the zonally averaged velocity and density fields to a basic state corresponding to the initial state.

Results described in the next sections concern the characteristics of the statistically equilibrated turbulent eddy field near the surface and within the interior. The mean Rossby number of this field (defined as $\sqrt{\langle \zeta^2 \rangle} / f_0$ with ζ the relative vorticity equal to $v_x - u_y$, with x and y (u and v), respectively, the zonal and meridional direction (velocity)) is large (close to 0.6) near the surface and smaller (close to 0.06) at 800 m.

Figure 2 shows snapshots of the relative vorticity fields at surface and 800 m. The surface relative vorticity field reveals a much stronger variability at submesoscale (as small as 8–20 km) consisting of numerous small-scale vortices as well as thin filaments. Relative vorticity extrema reach at the surface $3f$ and $-f$. At 800 m, the relative vorticity field displays a different spatial heterogeneity, dominated by larger vortices (>100 km) and thicker filaments, with magnitudes smaller than $0.4f$.

3. Review of the surface and interior properties

Properties reviewed in this section are fully described in Klein *et al.* (2008), Roulet and Klein (2009), Roulet and Klein (2010) and Lapeyre *et al.* (2006) (LKH06). They concern the horizontal and vertical kinetic energy as well as the ageostrophic effects (related to the divergent motions) on the cyclone/anticyclone asymmetry, the asymmetry of the isopycnal vertical displacements and the restratification/destratification.

3.1. Spectral characteristics of the kinetic energy

The KE distribution with depth (not shown) displays a significant surface intensification with almost 50% of this energy contained within the first 500 m.

Figure 3(a) shows the horizontal velocity spectra as a function of depth. At all depths, KE peaks at mesoscale (around 350–400 km). Within this scale range, the KE appears to be captured by the first baroclinic mode. Small scales (<60 km) are energetic only in the upper layers and weakens very rapidly as depth increases. The spectrum slopes exhibit these significant differences (Klein *et al.* 2008): near the surface, a noticeable shallow ($\approx k^{-2}$) spectrum slope is observed over a large spectral band (up to 300 km) indicating a continuous inertial range between small scales and mesoscales. At 800 m the velocity spectrum is much steeper with a slope close to k^{-4} for the same spectral range. Figure 3(a) further reveals some conspicuous discontinuities of the depth variations of the spectral slope (around 250 m and 800 m) that suggest three distinct regimes related to the small scales. One regime concerns the first 250 m where small scales are quite energetic. The other one, between 250 m and 800 m, where the energy of the small scales seems almost constant and the last one (below 800 m), where this energy quickly drops down.

Figure 3(b) shows the horizontal spectrum as a function of depth of the vertical velocity w . Near the surface the vertical KE is large in both mesoscale and small scale regions with a very significant contribution from the small scales (more than 50%, see Klein *et al.* (2008)). The vertical velocity field in this small-scale range has been found to be associated to the small-scale surface frontogenesis (Lapeyre *et al.* 2006). At depth, the spectrum reveals that the vertical KE is located principally at mesoscale. Figure 3(b) does not reveal any discontinuity of the spectrum slope with depth as those observed

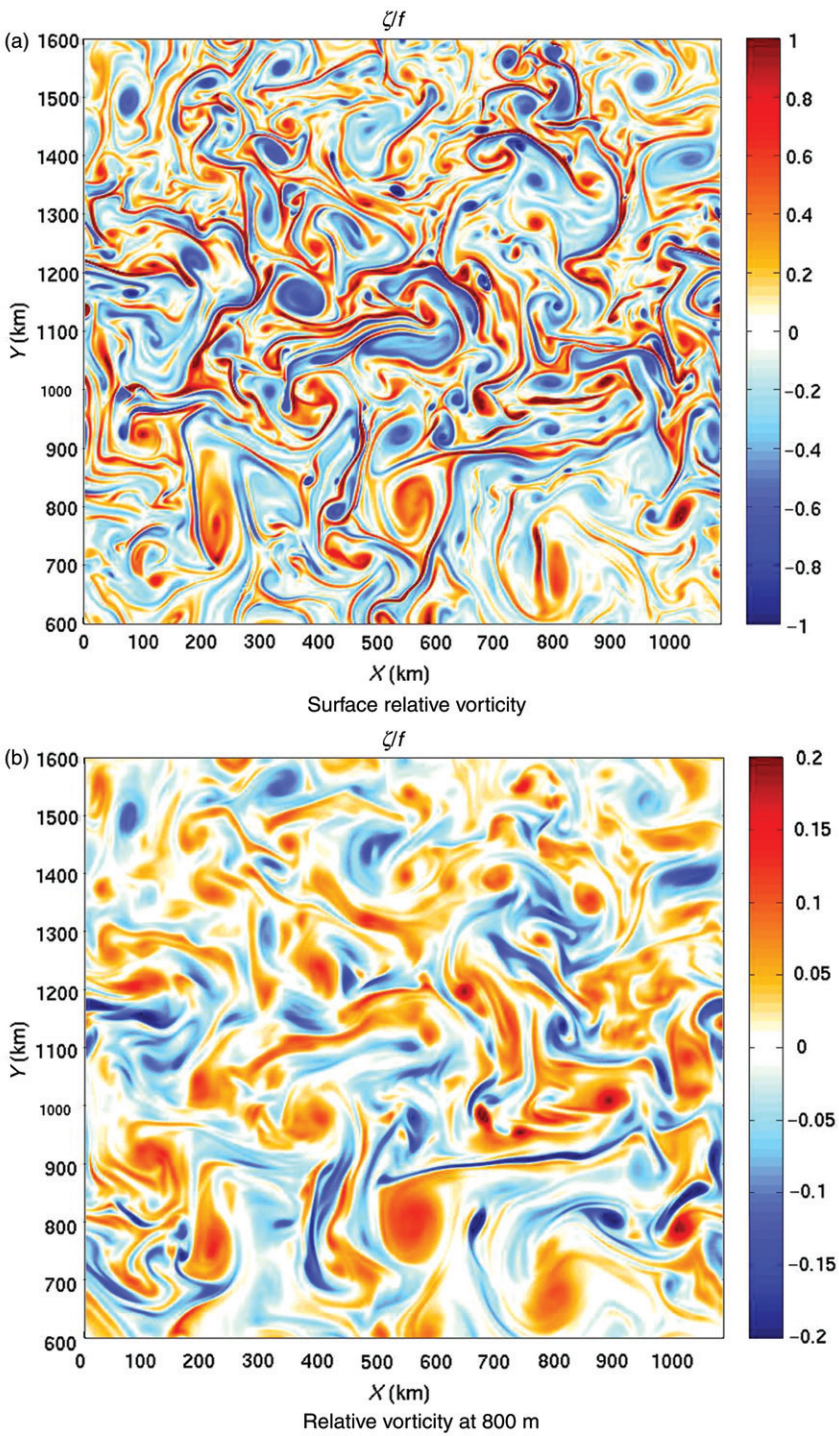


Figure 2. Snapshots of ζ/f . Note that the colorscale in (a) is symmetric and restricted to the range $[-f+f]$ in order to highlight both cyclonic and anticyclonic structures. In (b), the colorscale is divided by 5.

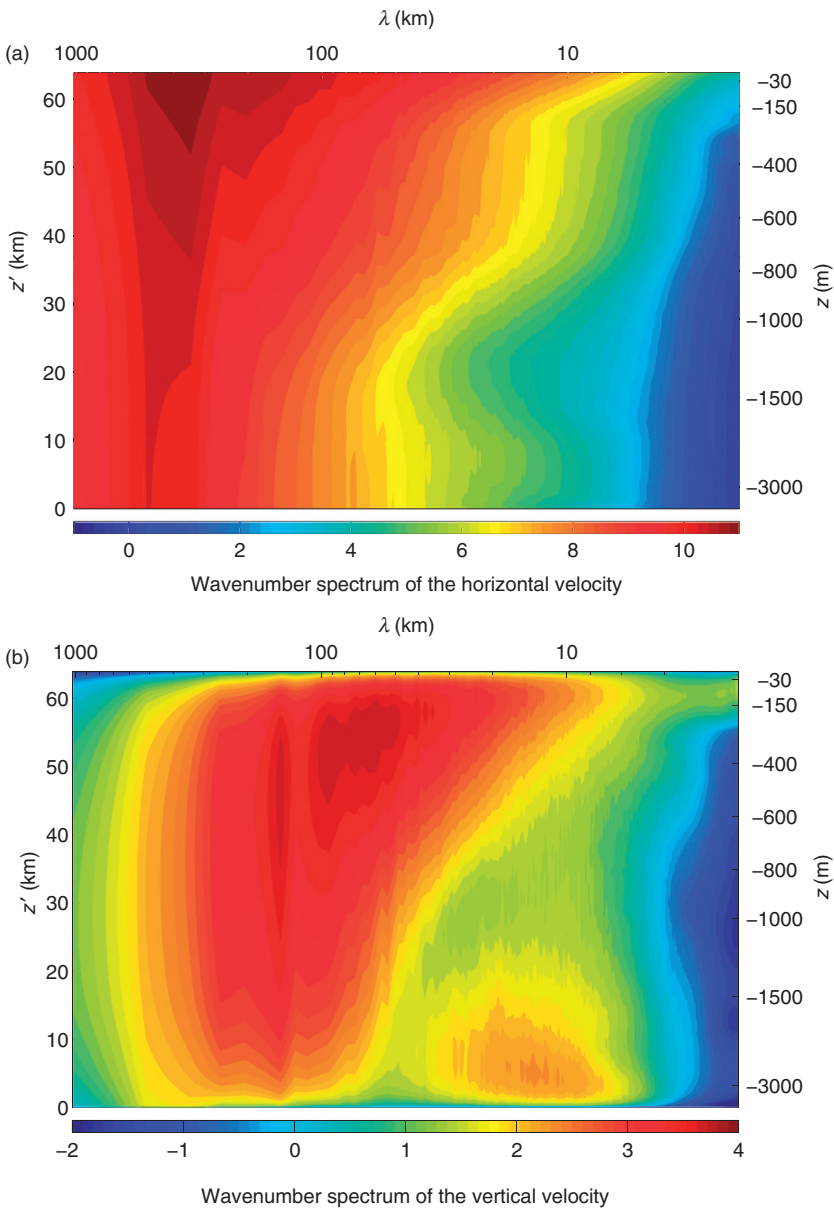


Figure 3. Wavenumber spectra (with wavelength indicated on top), as function of stretched vertical coordinate z' (left) and depth (right). Colorscales in (a) and (b) refer to the \log_{10} of the quantities plotted.

on figure 3(a). Below 1500 m, stratification becomes quite small, which does not inhibit w as much as it does in the upper layers. Note that a secondary maximum is observed at submesoscale around 3000 m. Results of Danioux *et al.* (2008) (that analyzed the vertical propagation of wind-forced near-inertial waves in a turbulent flow) strongly suggest that this secondary maximum present in this simulation with no wind forcing is explained in terms of near-inertial waves emitted by the turbulent flow.

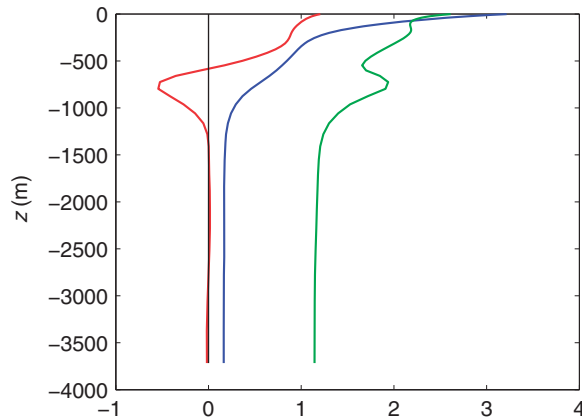


Figure 4. Statistics of ζ/f as a function of depth. Blue curve: rms (multiplied by 5); red curve: skewness; green curve: kurtosis (divided by 3) (adapted from Roulet, G. and Klein, P., Cyclone-anticyclone asymmetry in geophysical turbulence. *Phys. Rev. Lett.* 2010, **104**, doi: 10.1103/PhysRevLett.104.218501).

3.2. Cyclone/anticyclone asymmetry

A well-known prominent departure from SQG/QG flows is the emergence of vortical asymmetry. This vortical asymmetry has been explored by Roulet and Klein (2010) through the examination of the statistics of the relative vorticity as a function of depth. Vorticity skewness (red curve on figure 4) displays almost constant positive values (larger than 1) from the upper boundary down to 350 m. Then the skewness linearly decreases, to attain 0 at 600 m, and conspicuously becomes negative between 600 m and 1100 m (with a minimum equal to -0.4 at 800 m). Values below 1000 m are meaningless since the kinetic energy quickly drops down (Klein *et al.* 2008, Roulet and Klein 2010). Large positive skewness values as well as negative ones are accompanied by a local increase of the kurtosis (green curve on figure 4). In summary, a significant dominance of cyclonic structures is found over a large depth (400 m) whereas anticyclonic structures dominate below 600 m.

These results are consistent with those described in the literature. Hakim *et al.* (2002) using an SQG+1 model (i.e. an SQG model extended for Rossby number of order one) found a dominance of cyclonic structures in surface layers. Such asymmetry is explained in terms of the ageostrophic effects associated with small-scale surface frontogenesis (Hakim *et al.* 2002, McWilliams *et al.* 2009). On the other hand, anticyclonic dominance was reported by Polvani *et al.* (1994) using a shallow water model that mimics the behavior of baroclinic modes associated to the interior dynamics (with therefore no surface density anomaly) for large Rossby number. A similar result was found recently by Koszalka *et al.* (2009) from a PE simulation of ocean turbulence with no surface density anomaly. Polvani *et al.* (1994) pointed out that large Froude numbers (or small Burger numbers) enhance anticyclonic dominance.

In the present high-resolution simulations the ageostrophic effects associated with small-scale frontogenesis appear to explain the cyclone dominance in the surface layers (Roulet and Klein 2010). Impact of the vortex stretching may explain our observed anticyclone dominance in the interior. But there is still some work to do to fully explain this anticyclone dominance.

3.3. Restratification/destratification

Another prominent departure from SQG/QG of flows with large Rossby number is the change of the Brunt–Väisälä frequency. This property was highlighted by Hakim *et al.* (2002) using a SQG+1 model and fully explained by LKH06 using Ertel PV arguments. Such departure emerges in our simulations as shown by figure 5(a) (see also Klein *et al.* 2008).

The comparison of the mean density profile at equilibrium with that at initial time (figure 5(a)) corresponds, in terms of temperature change, to a warming of the first 350 m and a cooling of the deeper layers, between 350 m and 800 m. The warming corresponds to a surface temperature increase of almost one Celsius degree.

Mechanisms that trigger such departure in the upper layers from SQG/QG flows, are explained by LKH06 in terms of the ageostrophic effects related to the surface frontogenesis and to the vortex stretching in the interior. They are further discussed in section 4.

3.4. Isopycnal displacement asymmetry

A last prominent departure from SQG/QG flows is the asymmetry of the vertical displacements of the isopycnals (or asymmetry of the APE, also called anharmonic effects by (Roulet and Klein 2009)). The APE expression in terms of vertical displacements of the isopycnals (defined as for $\Delta z = z - z_r(\rho)$, where $\rho_r(z)$ is the density reference state and $z_r(\rho)$ its inverse mapping) is obtained by using a Taylor series expansion in $\Delta z = z - z_r(\rho)$ assuming the smallness of Δz) (Roulet and Klein 2009),

$$e_a(z, \rho) = -\frac{g}{2}\partial_z\rho_r\Delta z^2 - \frac{g}{6}\partial_{zz}^2\rho_r\Delta z^3 + O(\Delta z^4) \quad (1)$$

The second-order term (proportional to the isopycnal displacement variance) on the right-hand side (RHS) of (1) actually corresponds to the classical QG APE density (Pedlosky 1987). The third-order term on the RHS of (1) represents the departure from QG flows and can be interpreted in terms of the isopycnal displacement skewness. It is proportional to the curvature of the reference density profile and is the one referenced as the anharmonic effects ($e_{\text{anh}} \approx -(g/6)\partial_{zz}^2\rho_r\Delta z^3$) by Roulet and Klein (2009). Thus, large anharmonic effects are, therefore, associated with a significant skewness or asymmetry of the vertical displacements Δz .

Figure 5(b) reveals that e_{anh} is positive in the first 300 m below the surface and negative between 300 m and 700 m. Because of the positive sign of the density curvature in the first 300 m, positive e_{anh} indicates a negative skewness for the isopycnal displacements (downward displacements are more intense than upward ones). Given the results of section 3.2 one can conclude that, using PV conservation, this negative skewness is consistent with the cyclone dominance found in these upper layers. An opposite situation emerges below 400 m with a minimum of (negative) e_{anh} at 600 m. But these depths do not exactly coincide with those where anticyclone dominance is observed (i.e. between 600 m and 1000 m). The impact of the curvature variations of the reference density profile (see figure 5(a)) at those depths must not be negligible. Work is still under progress to fully relate these negative e_{anh} values to the observed anticyclone dominance found there. These asymmetric effects have been found to be quite small for small horizontal scales but significant at mesoscales.

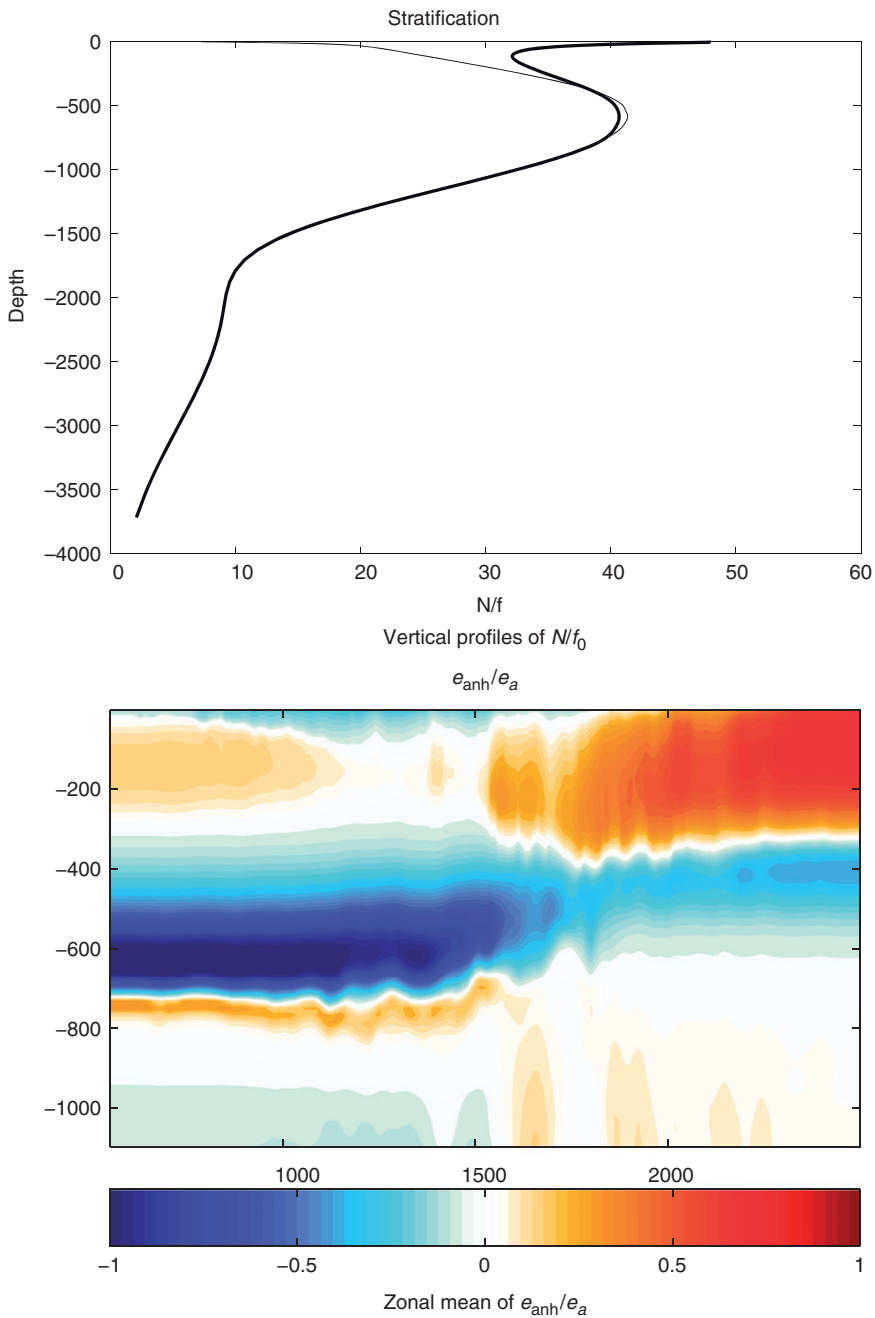


Figure 5. (a) Vertical profile of N/f_0 at the initial time (thin curve) and at the equilibrium (thick curve) (from Klein, P., Hua, B.L., Lapeyre, G., Capet, X., Le Gentil, S. and Sasaki, H., Upper ocean dynamics from high 3-D resolution simulations. *J. Phys. Oceanogr.* 2008, **38**, 1748–1763. © American Meteorological Society. Reprinted with permission.); (b) vertical meridional section of the zonal mean of e_{anh}/e_a with the depth (in m) on the vertical axis and the meridional distance (in km) on the horizontal axis (from Roulet, G. and Klein, P., Available potential energy in a direct numerical simulation of rotating turbulence. *J. Fluid Mech.* 2009, **624**, 45–55. Reproduced with permission from Cambridge, University Press).

4. Connection between surface and interior dynamics

Review of section 3 suggests that surface frontogenesis and SQG+1 explains a large part of the upper layer properties, due to the divergent motions, observed in numerical simulations (LK06, Capet *et al.* 2008a, Klein *et al.* 2008). For the interior, some interpretation begins to emerge, using arguments of shallow water theory (Polvani *et al.* 1994, Koszalka *et al.* 2010). But the depth transition between these two regimes is still unclear suggesting a more complex interaction between surface and interior dynamics than previously anticipated by LK06 and Tulloch and Smith (2009).

4.1. Phase locking between the surface and the interior in spectral space

A strong correlation in spectral space between surface and interior dynamical quantities was anticipated by LK06 within the QG framework. This can be demonstrated by inverting the Potential Vorticity (PV) equation

$$\nabla^2 \psi + \frac{\partial}{\partial z} \left(\frac{f_0^2}{N^2} \frac{\partial \psi}{\partial z} \right) = PV', \quad (2)$$

with the surface boundary conditions

$$-\frac{\rho_0 f_0}{g} \frac{\partial \psi}{\partial z} \Big|_{z=0} = \rho' \Big|_{z=0} . \quad (3)$$

with ψ the streamfunction, f_0 the Coriolis frequency, ρ' the density anomaly and N the Brunt–Väisälä frequency. ∇ is the horizontal gradient and z the vertical coordinate. Here PV' are the PV anomalies from the large-scale planetary PV. Inversion of this equation allows to get the streamfunction ψ at any depths and, therefore, the density ρ , the horizontal motions u and v and the vertical velocity w from, respectively, the hydrostaticity, the geostrophy, and the Omega equation.

LK06 split the problem (2) and (3) to two different problems in order to explicit the surface and interior contributions. The first one (noted int for interior) is forced by non-zero PV in the interior and involves zero surface density:

$$\nabla^2 \psi_{\text{int}} + \frac{\partial}{\partial z} \left(\frac{f_0^2}{N^2} \frac{\partial \psi_{\text{int}}}{\partial z} \right) = PV' \quad (4a)$$

with

$$-\frac{\rho_0 f_0}{g} \frac{\partial \psi_{\text{int}}}{\partial z} \Big|_{z=0} = 0 . \quad (4b)$$

The second one (noted sur for surface) involves zero PV in the interior and is forced by non-zero surface density:

$$\nabla^2 \psi_{\text{sur}} + \frac{\partial}{\partial z} \left(\frac{f_0^2}{N^2} \frac{\partial \psi_{\text{sur}}}{\partial z} \right) = 0 \quad (5a)$$

with

$$-\frac{\rho_0 f_0}{g} \frac{\partial \psi_{\text{sur}}}{\partial z} \Big|_{z=0} = \rho' \Big|_{z=0}. \quad (5b)$$

The total streamfunction field is, therefore, given by the sum of the two contributions $\psi = \psi_{\text{int}} + \psi_{\text{sur}}$. When the mean meridional density gradient has a vertically correlated structure, one may write, as in LK06,

$$\bar{\rho}(y, z) \approx \bar{\rho}_s(y) F(z) \quad (6)$$

with $F(z) = 1$ at $z = 0$. Hereafter, the bar denotes the zonal average. If the mean PV gradient is dominated by the stretching term, we can write

$$\frac{\partial \overline{PV}}{\partial y} \approx -\frac{g}{\rho_0 f_0} \alpha(z) \frac{\partial \bar{\rho}_s}{\partial y} \quad (7a)$$

with

$$\alpha(z) = \frac{\partial}{\partial z} \left(\frac{f_0^2 F(z)}{N(z)^2} \right). \quad (7b)$$

Then, conservation of potential vorticity and surface density lead to

$$PV'(x, y, z) \approx -\frac{g}{\rho_0 f_0} \alpha(z) \rho'_s(x, y). \quad (8)$$

Integrating (4) to (5) using (8) shows that the horizontal structure of ψ_{int} will be phase-locked with the horizontal structure of ψ_{sur} . Only their vertical dependence will be different. Indeed, assuming a constant stratification for the sake of simplicity (generalization to N^2 depth dependent is immediate) and moving to the spectral space (using $\widehat{\cdot}$ the Fourier transform and k the modulus of the wavenumber vector, $k = |\mathbf{k}|$), the solutions,

$$\widehat{\psi}_{\text{int}} = \frac{g}{\rho_0 f_0} \frac{\alpha(z)}{k^2 + (f_0^2 / (N^2 H^2))} \widehat{\rho}'_s, \quad (9a)$$

$$\widehat{\psi}_{\text{sur}} = -\frac{g}{\rho_0 f_0} \frac{f_0}{kN} \exp\left(\frac{kNz}{f_0}\right) \widehat{\rho}'_s \quad (9b)$$

(with H the total depth) indicate that ψ_{int} and ψ_{sur} have the same phase as ρ_s .

If we introduce h_c the Charney scale (Held 1978) as

$$h_c = \frac{g f_0}{\rho_0 N^2} \frac{\partial_y \bar{\rho}_s}{\partial_y \overline{PV}}. \quad (10)$$

Using (7a) we obtain $\alpha(0) = f_0^2 / h_c N^2$. Usually we have $h_c \ll H$ (Held 1978). From (9), solutions are equal near the surface for a critical wavenumber k_c such that $\alpha(0) / (k^2 + (f_0^2 / (N^2 H^2))) = f_0 / kN$, which corresponds (using $h_c \ll H$) to $k_c \approx \alpha(0)N / f_0 = f_0 / Nh_c$. Then, from (9), the interior QG solution dominates for wavenumbers smaller than k_c , whereas the surface QG solution dominates for wavenumber larger than k_c . This critical wavenumber is the same as that found by Smith and Tulloch (2009) although our analytical approach is different.

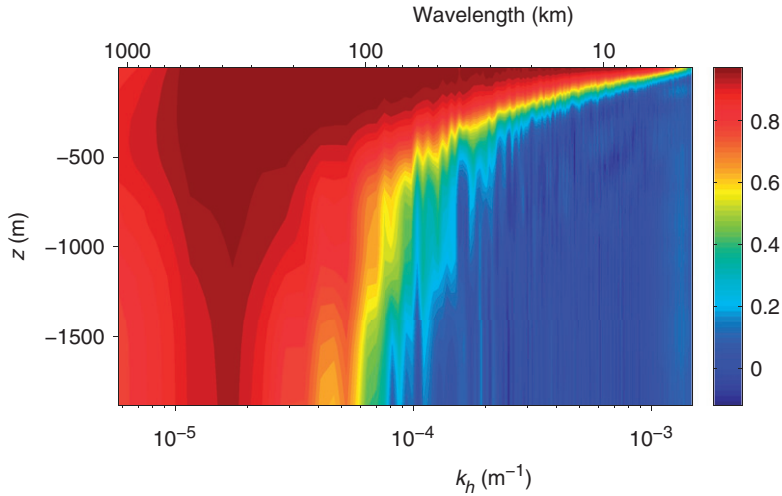


Figure 6. Spectral correlation between the surface relative vorticity and the relative vorticity at depth.

We may wonder whether this phase relationship still exists for flows with $O(1)$ Rossby number. Figure 6 shows the spectral correlation between surface relative vorticity and vorticity in the interior. Such spectral correlation is calculated as $\text{Re}[\widehat{\zeta}(\mathbf{k}, 0) \cdot \widehat{\zeta}^*(\mathbf{k}, z)] / |\widehat{\zeta}(\mathbf{k}, 0)| |\widehat{\zeta}(\mathbf{k}, z)|$ (with $(\cdot)^*$ standing for the complex conjugate and Re the real part) and therefore is simply related to the cosine of the phase difference between $\widehat{\zeta}(\mathbf{k}, 0)$ and $\widehat{\zeta}(\mathbf{k}, z)$. We can see from figure 6 that, for a given wavenumber, the spectral correlation is very good down to a depth that depends on the wavenumber magnitude. This depth dependence has been shown in our simulations to be quite close to that expressed in (9) (Klein *et al.* 2009). A similar spectral correlation is observed between the surface and interior density. Indeed scales of the order of $O(50)$ km are correlated (and phase-locked) down to a depth not larger than 500 m, but scales of $O(200)$ km are correlated down to 1000 m. Figures 3(a) and 6 further indicate that mesoscales are equivalent barotropic. Thus although our flow dynamics well depart from QG dynamics, as shown in previous sections, the phase-locking between surface and interior dynamical quantities still exists.

Although this phase-locking appears inherent to the chosen vertical structure of the mean density gradient, it is worth to note that it has been well observed in realistic simulations of the North Atlantic (in particular, in the Gulf Stream region (Isern-Fontanet *et al.* 2008, Lapeyre 2009)), which implies a strong coherence between surface and interior dynamics in this region. Such phase-locking also emerges from the analysis of mooring data in high kinetic energy regions (Ferrari and Wunsch 2010).

4.2. Connection between surface and interior divergent motions through mass conservation

LKH06 pointed out, using Ertel PV arguments that the time evolution of the density field averaged horizontally is driven at any depths by the following equation

$$\frac{\partial \langle \rho \rangle}{\partial t} = -\frac{1}{f_0} \left(\frac{\partial \langle \rho \zeta \rangle}{\partial t} + \langle wQ \rangle \right), \quad (11)$$

where $\langle \rangle$ denotes the horizontal spatial averaging operator and \mathcal{Q} is the Ertel PV. Integrating (11) over depth and using mass conservation leads to an equality between the two RHS terms (LKH06). LKH06 further showed that the first RHS term is strongly dominated by the contribution of $\langle w_z \rho \rangle$ and forced by the surface frontogenesis at small-scale. The second RHS term is dominated by the vertical advection of the stretching associated with the mesoscale eddies (i.e. $\langle w \rho_z \rangle$). LKH06 results, using free decaying turbulence simulations with constant stratification, indicate that, with zero surface density anomalies (leading to no surface frontogenesis), the first RHS term is smaller than the second one over the whole depth and therefore, the second RHS term (dominated by $\langle w \rho_z \rangle$) displays a sign change on the vertical because of the mass conservation constraint (and in particular because $\int_{-H}^0 \langle w_z \rho \rangle dz + \int_{-H}^0 \langle w \rho_z \rangle dz = 0$). On the other hand, with non-zero surface density anomalies the first RHS term is very large in the upper layers (much larger than the second RHS term), because of the energetic surface frontogenesis, and mostly positive over the whole depth. They showed that, as a consequence, the second term has to adjust to satisfy the mass conservation constraint and therefore becomes negative over the whole water column. They concluded that surface frontogenesis has a significant impact on the interior vortex stretching.

Figure 7 clearly indicates that, in the present higher resolution and more realistic (than in LKH06) simulations of ocean turbulence, the contribution of $\langle w_z \rho \rangle$ (and therefore of the first RHS term in (11)) is very large in the surface layers and mostly positive. On the other hand, $\langle w \rho_z \rangle$ (and therefore, the second RHS term) has smaller magnitude in the upper layers and is mostly negative over the whole depth. To further highlight the impact of an active surface boundary, we performed additional simulations similar to the previous ones but with the large-scale meridional density gradient set to zero very close to the surface boundary (such that there is no surface density anomaly and, therefore, no surface frontogenesis). Although the KE is still intensified in the first 500 m with almost the same magnitude, the vertical profiles of

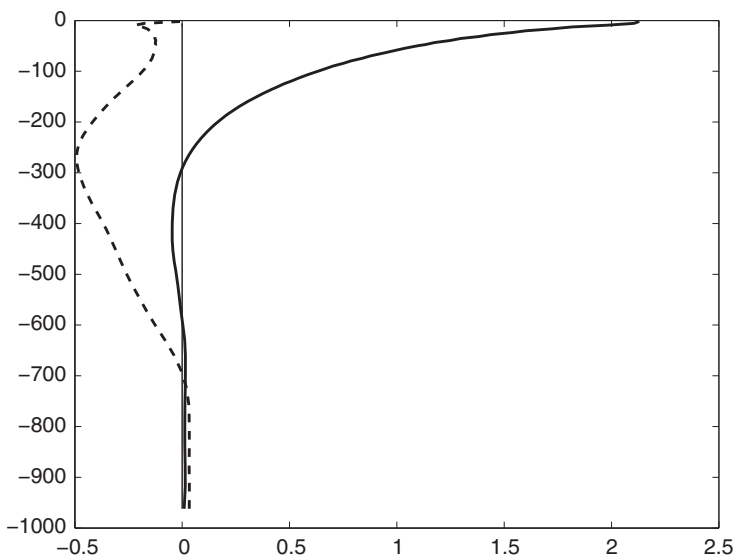


Figure 7. Vertical profiles of $\langle w_z \rho \rangle$ (solid line) and of $\langle w \rho_z \rangle$ (dashed line).

$\langle w_z \rho \rangle$ and $\langle w \rho_z \rangle$ (not shown) are very different from those of figure 7 and quite similar to those reported by LKH06 with no surface density anomaly. These new results suggest similar conclusions as those of LKH06, i.e. the interior vortex stretching is strongly connected to the surface frontogenesis.

4.3. Surface kinetic energy budget: role of the surface divergent motions

An additional suggestion of this two-way connection driven by the divergent motions is given by the surface kinetic energy (KE) budget that, in spectral space, is

$$\frac{1}{2} \frac{\partial |\widehat{\mathbf{u}}_h|^2}{\partial t} = -\text{Re}(\widehat{\mathbf{u}}_h^* \cdot \widehat{(\mathbf{u}_h \cdot \nabla_H \mathbf{u}_h)}) - \frac{1}{\rho_0} \text{Re}(\widehat{w}_z^* \widehat{p}), \quad (12)$$

with \mathbf{u}_h the horizontal velocity field, ∇_H the horizontal gradient operator, and p the pressure. This budget involves two dominant terms: the advection term that is responsible for the inverse KE cascade through the nonlinear interactions and the pressure term associated to a transfer of APE into KE. Additional mixing terms (not discussed here) include vertical and horizontal mixing. Figure 8 shows the integral KE budget terms. These terms are just the integral of the local budget terms over the spectral wavenumber range $[k, \infty]$, i.e. $\Pi_A(k) = \int_k^\infty A(k) dk$ with A one of the terms in (12).

Discussion of these budget terms is fully developed in Klein *et al.* (2008). For the purpose of the present study let us notice that the advection term (Π_u ; solid curve on figure 8) is mostly negative over a large spectral range ($k > 10$), which indicates a dominant inverse nonlinear transfer (or cascade) of KE within the range between 300 km and 30 km. The pressure term (Π_p ; dashed curve on figure 8) is positive over the whole spectral range. Since it is linked to the horizontal velocity divergence, its contribution as a source (especially within the small-scale range) indicates that it is

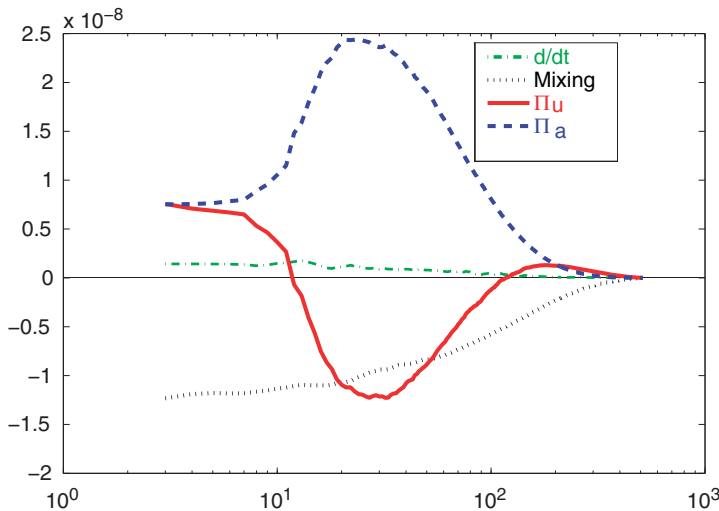


Figure 8. Integral budget for the surface KE. Horizontal axis display the nondimensional wavenumber k . The value $k=10$ corresponds to a wavelength of 300 km. Units on the vertical axis are in $\text{m}^2 \text{s}^{-3}$. Adapted from Klein, P. Hua, B.L., Lapeyre, G., Capet, X., Le Gentil, S. and Sasaki, H., Upper ocean dynamics from high 3-D resolution simulations. *J. Phys. Oceanogr.* 2008, **38**, 1748–1763. © American Meteorological Society. Reprinted with permission.

mostly driven by small-scale frontogenesis. Positiveness of this term has been explained in terms of restoration of the thermal wind balance in Klein *et al.* (2008) and Capet *et al.* (2008c). It partly compensates for the KE advective term. This pressure term has also been interpreted as a transformation of APE into KE at small scales through frontogenesis (Capet *et al.* 2008b, c). The impact of the small scales on these two terms has been further noted by (Capet *et al.* 2008b): when the resolution increases by a factor two, the amplitude of each term is multiplied by a factor almost equal to two. This strengthens the result obtained in Capet *et al.* (2008c) indicating that, at the surface, small-scale frontogenesis (and the related divergent motions) is the principal mechanism that transforms APE into KE at small scales with this KE then being transferred towards larger scales through the inverse KE cascade.

This result about the importance of the small-scale frontogenesis for the energy transformation at the surface is consistent with the positive and very large amplitude of the term $\langle w_z \rho \rangle$ in the surface layers found in the preceding section. Combined with that of section 4.2, this result suggests that the small-scale surface frontogenesis mechanisms (and mostly their divergent motions) not only efficiently transfer, at the surface, a part of APE into KE (then transferred at the surface to larger scales through the inverse cascade) but also affect the vertical structure of these mesoscales through their effects on the vortex stretching in the interior. At last, these two results appear to be consistent with the phase-locking between the surface and the interior in spectral space discussed in section 4.1.

5. Conclusion

Analysis of recent high-resolution simulations of ocean turbulence with large Rossby number clearly suggests a close interaction between the surface dynamics and the interior dynamics for which the contribution of surface-trapped submesoscales, ubiquitous on infrared and ocean color satellite images, appears to be significant. On one hand, these submesoscales are produced by the horizontal stirring of surface density anomalies by mesoscale eddies (with larger depth extension). On the other hand, the divergent motions associated with these submesoscales impact the mesoscale eddy dynamics. Indeed these divergent motions (triggered by the frontogenesis mechanisms) are involved in the APE transfer into KE at the surface and as such submesoscales feed up surface mesoscale eddies through the inverse KE cascade. Furthermore, these divergent motions are closely connected with the eddy vortex stretching at depths through the constraint of the mass conservation, which preserves their vertical phase relationship. Such energy transfers favored by the energetic small-scale divergent motions may explain the larger kinetic energy displayed by ocean turbulence simulations when the resolution is higher.

These results emphasize the importance of taking into account explicitly the small-scale frontogenesis mechanisms, and the related divergent motions, in the upper layers in order to represent the full nonlinear interactions and, therefore, the properties of the oceanic turbulence. High spatial resolution, consistent in both horizontal and vertical directions, is a prerequisite to represent the dynamics of these small-scale structures.

Acknowledgements

Discussions with Bach Lien Hua and Xavier Capet (coauthors of some of the papers reviewed in this study) are warmly acknowledged. This work is supported by IFREMER and CNRS (FRANCE). Numerical simulations reported here were done on the Earth Simulator (Yokohama, Japan) whose access has been possible through a M.O.U. signed between IFREMER, CNRS, and JAMSTEC. Patrice Klein, Guillaume Rouillet and Sylvie Le Gentil also acknowledge the support from the French ANR (Agence Nationale pour la Recherche, Contract no ANR-05-CIGC-010).

References

- Abraham, E.R., Law, C.S., Boyd, P.W., Lavender, S.J., Maldonado, M.T. and Bowle, A.R., Importance of stirring in the development of an iron-fertilized phytoplankton bloom. *Nature* 2000, **407**, 727–730.
- Blumen, W., Uniform potential vorticity flow: part I. Theory of wave interactions and two-dimensional turbulence. *J. Atmos. Sci.* 1978, **35**, 774–783.
- Capet, X., Klein, P., Hua, B.L., Lapeyre, G. and McWilliams, J., Surface kinetic and potential energy transfer in SQG dynamics. *J. Fluid Mech.* 2008c, **604**, 165–174.
- Capet, X., McWilliams, J.C., Molemaker, M.J. and Shchepetkin, A.F., Mesoscale to submesoscale transition in the California current system. Part 1: flow structure and Eddy flux. *J. Phys. Oceanogr.* 2008a, **38**, 29–43.
- Capet, X., McWilliams, J.C., Molemaker, M.J. and Shchepetkin, A.F., Mesoscale to submesoscale transition in the California current system. Part 3: energy balance and flux. *J. Phys. Oceanogr.* 2008b, **38**, 2256–2269.
- Chelton, D.B., Schlax, M.G., Samelson, R.M. and De Szoeke, R.A., Global observations of large ocean eddies. *Geophys. Res. Lett.* 2007, **34**, L15606.
- Danioux, E., Klein, P. and Rivière, P., Propagation of wind Energy into the deep ocean through mesoscale eddies. *J. Phys. Oceanogr.* 2008, **38**, 2224–2241.
- Ferrari, R. and Wunsch, C., The distribution of eddy kinetic and potential energies in the global ocean. *Tellus* 2010, **62**, 92–108.
- Hakim, G.J., Snyder, C. and Muraki, D.J., A new surface model for cyclone-anticyclone asymmetry. *J. Atmos. Sci.* 2002, **59**, 2405–2420.
- Held, I.M., The vertical scale of an unstable baroclinic wave and its importance for eddy heat flux parameterizations. *J. Atmos. Sci.* 1978, **35**, 572–576.
- Isern-Fontanet, J., Lapeyre, G., Klein, P., Chapron, B. and Hecht, M., Ocean dynamics reconstruction from surface information. *J. Geophys. Res.* 2008, **113**, C09005.
- Klein, P., Hua, B.L., Lapeyre, G., Capet, X., Le Gentil, S. and Sasaki, H., Upper ocean dynamics from high 3-D resolution simulations. *J. Phys. Oceanogr.* 2008, **38**, 1748–1763.
- Klein, P., Isern-Fontanet, J., Lapeyre, G., Rouillet, G., Danioux, E., Chapron, B., Le Gentil, S. and Sasaki, H., Diagnosis of vertical velocities in the upper ocean from high resolution sea surface height. *Geophys. Res. Lett.* 2009, **36**, L12603, 1–5, doi:10.1029/2009GL038359.
- Koszalka, I., Bracco, A., McWilliams, J.C. and Provenzale, A., Dynamics of wind-forced coherent anticyclones in open ocean. *J. Geophys. Res.* 2009, **114**, C08011.
- Koszalka, I., Ceballos, L. and Bracco, A., Vertical mixing and coherent anticyclones in the ocean: the role of stratification. *J. Geophys. Res.* 2010, **17**, 37–47.
- Lapeyre, G., What mesoscale signal does the altimeter reflect? On the decomposition in baroclinic modes and on a surface-trapped mode. *J. Phys. Oceanogr.* 2009, **39**, 2857–2874.
- Lapeyre, G. and Klein, P., Dynamics of the upper oceanic layers in terms of surface quasigeostrophic theory. *J. Phys. Oceanogr.* 2006, **38**, 165–176.
- Lapeyre, G., Klein, P. and Hua, B.L., Oceanic restratification by surface frontogenesis. *J. Phys. Oceanogr.* 2006, **36**, 1577–1590.
- Le Traon, P.Y., Klein, P., Hua, B.L. and Dibarboure, G., Do altimeter data agree with interior or surface quasi-geostrophic theory. *J. Phys. Oceanogr.* 2008, **38**, 1137–1142.
- McGillicuddy, D.J., Robinson, A.R., Siegel, D.A., Jannasch, H.W., Johnson, R., Dickey, T.D., McNeil, J., Michaels, A.F. and Knap, A.H., Influence of mesoscale eddies on new production in the Sargasso Sea. *Nature* 1998, **394**, 263–266.

- McWilliams, J.C., Colas, F. and Molemaker, M.J., Cold filamentary intensification and oceanic surface convergence lines. *Geophys. Res. Lett.* 2009, **36**, L18602.
- Pedlosky, J., *Geophysical Fluid Dynamics*, 1987. (New York: Springer-Verlag).
- Polvani, L.M., McWilliams, J.C., Spall, M.A. and Ford, R., The coherent structures of shallow-water turbulence: deformation-radius effects, cyclone/anticyclone asymmetry and gravity-wave generation. *Chaos* 1994, **4**, 177–186.
- Rivière, P., Treguier, A.M. and Klein, P., Effect of bottom friction on nonlinear equilibration of an oceanic baroclinic jet. *J. Phys. Oceanogr.* 2004, **34**, 416–432.
- Roullet, G. and Klein, P., Available potential energy diagnosis in a high-resolution model of rotating stratified turbulence. *J. Fluid Mech.* 2009, **624**, 45–55.
- Roullet, G. and Klein, P., Cyclone-anticyclone asymmetry in geophysical turbulence. *Phys. Rev. Lett.* 2010, **104**, 218501-1–218501-4, doi:10.1103/PhysRevLett.104.218501.
- Smith, K.S., Maltrud, M., Bryan, F. and Hecht, M., Numerical simulation of the North Atlantic Ocean at $1/10^\circ$. *J. Phys. Oceanogr.* 2000, **30**, 1532–1561.
- Smith, S.K. and Tulloch, R., Reply. *J. Atmos. Sc.* 2009, **66**, 1073–1076.
- Smith, K.S. and Vallis, G.K., The scales and equilibration of midocean eddies: forced-dissipative flows. *J. Phys. Oceanogr.* 2002, **32**, 1699–1721.
- Tulloch, R. and Smith, S.K., A new theory for the atmospheric energy spectrum: depth-limited temperature anomalies at the tropopause. *Proc. Nat. Am. Soc.* 2006, **103**, 14690–14694.
- Tulloch, R. and Smith, S.K., Quasigeostrophic turbulence with explicit surface dynamics: application to the atmospheric energy spectrum. *J. Atmos. Sc.* 2009, **66**, 450–467.